

# Studies of hyperon production in HADES — cascade production

Joanna Kuboś<sup>1</sup>  
for the HADES Collaboration

<sup>1</sup>Institute of Nuclear Physics PAS, Kraków, Poland,  
joanna.kubos@ifj.edu.pl

**Abstract.** Production of the doubly strange  $\Xi^-$  hyperon, known as a cascade particle, has been investigated in nuclear reactions in a wide energy range. However, only the results for the energies above the threshold for cascade production in elementary collisions were known for a long time. The first measurement of the subthreshold  $\Xi^-$  production was performed in heavy ion and nucleon-nucleus collisions by the HADES Collaboration. Because of the discrepancy between data and various model predictions deeper studies of the strangeness production, especially in elementary collisions near the threshold, are needed. In this paper simulations of the cascade production in proton-proton reaction at the beam kinetic energy of 4.5 GeV are presented. The results are relevant for the experiment planned by HADES with the upgraded setup during the FAIR-Phase0 project.

**Keywords:** cascade, strangeness production, transport models, HADES

## 1 Introduction

Processes of the strangeness production have been the subject of interest of nuclear physicists for a long time. Such studies are important for the investigations of the nuclear equation-of-state (EoS), neutron stars compositions or scattering processes in hot and dense matter. Especially the multistrange particles production yield, enhanced in nucleon-nucleus reactions in respect to the nucleon-nucleon, is a sign of the phase transition of the hadronic matter to the quark-gluon plasma state (QGP).

Production of cascade — a doublystrange  $\Xi^-$  hyperon — was measured by different experiments: in heavy ion collisions at LHC [1,2], RHIC [3,4], SPS [5,6] and AGS [7], in nucleon-nucleon collisions at LHC [8], in nucleon-nucleus reactions at DESY [9] and SPS [10] and also at lowest energy in HADES: Ar+KCl@1.76 AGeV [11] and p+Nb@3.5 GeV [12] (experimental data shown in the Fig. 1). The latter measurements have shown the enhanced  $\Xi^-$  production with respect to the model predictions (see Fig. 1). To describe the experimental data transport models are used [16,17,18,19,20].

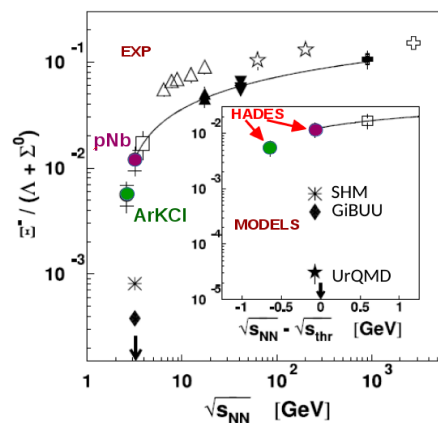


Fig. 1: The yield ratio  $\Xi^- / (\Lambda + \Sigma^0)$  as a function of  $\sqrt{s_{NN}}$  or  $\sqrt{s_{NN}} - \sqrt{s_{thr}}$  (inset). Full dots — data measured by HADES. (Figure from [12])

The cascade production in the HADES energy range was initially modeled as processes of strangeness-exchange:  $\bar{K}Y \rightarrow \pi\Xi$ , where  $Y = \Lambda, \Sigma$  [13]. However, the observed production of cascade in p+Nb reactions questions this hypothesis.

The unexpected high production rate of cascade in the Ar+KCl experiment [11] seems to be partially explained by adding an additional process to the UrQMD model — a hyperon-hyperon scattering  $YY \rightarrow N\Xi$  [14,15], but the theoretical  $\Xi^-$  abundance is still significantly lower than the experimental data. In the case of the p-Nb reaction differences between model predictions with and without  $YY$  scattering is negligible [12]. Therefore, a new mechanism of cascade production in the nucleon-nucleus interaction was proposed — subthreshold cascade production via high-mass baryon resonances [21].

To resolve this so called "HADES puzzle", i.e. the cascade overproduction near the threshold, and improve our knowledge about elementary processes responsible for the strangeness creation, it is necessary to measure the  $\Xi^-$  production in nucleon-nucleon collision in near-threshold energies.

In this letter result of simulations of the cascade production in elementary collisions:  $pp \rightarrow \Xi K^+ K^+ p$  at  $E = 4.5$  GeV will be presented.

## 2 HADES detector

HADES (**H**igh **A**cceptance **D**ielectron **S**pectrometer) is a versatile magnetic spectrometer [22]. Its main purpose is to detect dielectrons and hadrons in pion, proton and heavy-ion induced reactions. Geometrically the detector is divided into six sectors placed symmetrically around the beam axis. HADES consists of a Ring Imaging gas Cherenkov detector (RICH) for electron-hadron discrimination, a set of six superconducting coils producing a toroidal field, four sets of multiwire drift chambers (MDC) — two before and two after the magnetic field serving as a tracking system, and a multiplicity and electron trigger array consisting of: a time-of-flight wall (TOF) and a RPC wall and the new Electromagnetic Calorimeter (ECAL). Identification of the charged particles — pions, kaons and protons is achieved by combining time-of-flight and energy loss measurements over a large momentum range. The detector system covers 85% of the polar angle in the range from  $18^\circ$  to  $85^\circ$  with the momentum resolution  $\frac{\Delta p}{p} \approx 2 - 4\%$ .

The physics program of HADES is mostly focused on a studies of QCD matter phase diagramme in the region of the high baryonic potential, the investigation of hadron properties in nuclei and in the hot and dense hadronic matter.

### 2.1 Forward Detector

Currently the HADES detector is upgraded by the new and faster readout electronics (DAQ) and the Forward Detector for tracking in very forward angles, which extends the angular coverage of the detection setup to the forward angles  $\theta \in [0.5^\circ - 6.5^\circ]$ . A schematic picture of the upgraded HADES is shown in Fig. 2.

The cascade decay in HADES is measured in a two step decay process: (1)  $\Xi^- \rightarrow \Lambda\pi^-$ , (2)  $\Lambda \rightarrow p\pi^-$ . As one knows from the kinematics protons produced in the  $\Lambda$  decay are emitted in very forward angles (see Fig. 3). Therefore with the use of the currently operating HADES setup one is able to reconstruct only about 9% of all possible protons and, in consequence, only very small fraction of all cascade decays. To improve the count rate of the  $\Xi^-$  it is necessary to detect also the protons with scattering angles below  $\theta < 18^\circ$ . As a solution the Forward Detector has been proposed.

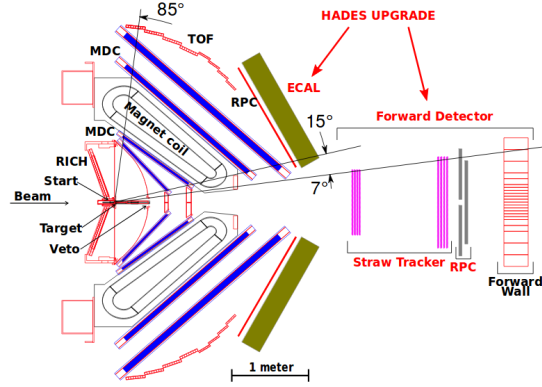


Fig. 2: Scheme of the upgraded HADES setup together with the Forward Detector.

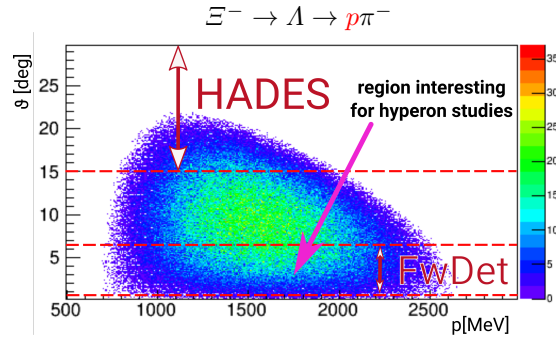


Fig. 3: Angular distribution of protons produced in the  $\Lambda$  decay, which is the second step of the cascade decay. The angular acceptance of the HADES detector before upgrade and of the Forward Detector is marked.

Forward Detector consists of two stations of Straw Tube Trackers (STS1 and STS2) for a precise particles tracking [23] and a set of Resistive Plate Chambers (RPC) for time-of-flight measurement. Due to the fact that the Forward Detector is placed in the region with no magnetic field full PID is not possible. Owing to this in the simulation scheme all charged particles detected in Forward Detector are treated as protons (the mass of such particles is fixed as proton mass).

### 3 Simulations and signal reconstruction

The cascade production channel:  $pp \rightarrow \Xi^- K^+ K^+ p$  as well as the most contributing background channels have been simulated with the use of the PLUTO Monte-Carlo event generator [24]. The simulated channels are listed in Tab. 1. The geometry and detector response have been simulated with the use of GEANT3-based software considering the upgraded HADES setup.

Table 1: List of the simulated reaction channels together with the cross-sections.

| No. | reaction                 | cross-section [ $\mu\text{b}$ ] |
|-----|--------------------------|---------------------------------|
| 0.  | $K^+K^+p\Xi^-$           | 4.8                             |
| 1.  | $pp2\pi^-2\pi^+$         | 600                             |
| 2.  | $p\Lambda K_s^0\pi^+$    | 100                             |
| 3.  | $p\Lambda K^+\pi^+\pi^-$ | 30                              |
| 4.  | $n\Lambda K_s^02\pi^+$   | 30                              |
| 5.  | $p\Sigma^0 K_s^0\pi^+$   | 20                              |
| 6.  | $pp2K_s^0$               | 20                              |

### 3.1 Steps of the analysis

The cascade is produced in  $pp$  reaction accompanied by two positive kaons and one proton.  $\Xi^-$  decays to the negative pion and the  $\Lambda$  ground state, which subsequently decays into proton and  $\pi^-$ . Detection of two negative pions in HADES and one charged particle in Forward Detector (treated as a proton) is considered as a candidate for the  $\Xi^-$  decay. In the first step the 4-momentum and the decay vertex of the  $\Lambda$  hyperon ( $\Lambda \rightarrow p\pi^-$ ) are reconstructed by the combination of a negative pion detected in HADES ( $\theta > 18^\circ$ ) with a proton detected in Forward Detector ( $\theta < 6.5^\circ$ ). Next, the same observables are calculated for  $\Xi^-$  ( $\Xi^- \rightarrow \Lambda\pi^-$ ) obtained from the momentum vectors of  $\Lambda$  reconstructed in the first step and another  $\pi^-$  detected in HADES (not used in the  $\Lambda$  reconstruction).

### 3.2 Topological cuts

During the analysis following topological cuts have been applied to reduce background: (1) Minimum Tracks Distance for  $\Lambda$  decay vertex (MTD\_L) — a value of the lower distance between  $p$  and  $\pi^-$  tracks:  $\text{MTD\_L} < 25$  mm; (2) the  $z$  coordinate of the secondary vertex (VERTz\_L); it is an estimated  $\Lambda$  decay vertex calculated as the middle point of the shortest section drawn between  $p$  and  $\pi^-$  tracks:  $\text{VERTz\_L} \in [-20;300]$  mm; (3) Minimum Tracks Distance for  $\Xi^-$  decay vertex (MTD\_X) — a value of the lower distance between reconstructed  $\Lambda$  and  $\pi^-$  tracks:  $\text{MTD\_X} < 20$  mm. The cuts applied are presented in Fig. 4 together with the optimized values.

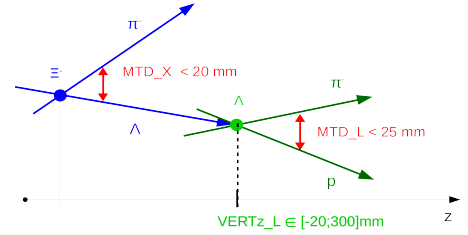


Fig. 4: The topological cuts applied to the cascade reconstruction.

### 3.3 Results

The results of the analysis are presented in Fig. 5. The two steps are shown: the reconstruction of the invariant mass of  $p\pi^-$  (left panel) and  $\Lambda\pi^-$  (after a cut on  $\Lambda$  peak in  $p\pi^-$  invariant mass) (right panel). As a signal (green solid line) events in the range of  $\pm 3\sigma$  from the peak position have been

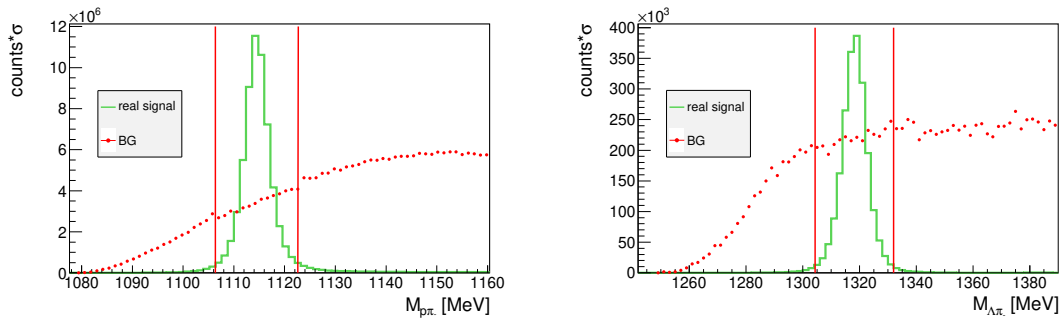


Fig. 5: Reconstructed signal of  $\Lambda$  (*left panel*) and cascade (*right panel*) — green solid line and sum of the background reactions — red dotted line. Vertical lines —  $\pm 3\sigma$  of the invariant mass peak.

accepted. Red dotted line represents appropriately normalized sum of all considered background reactions (see Tab. 1).

The count rate for the reaction of cascade production in  $pp$  scattering at  $E=4.5$  GeV considering the upgraded HADES setup (beam rate =  $10^8$  part/s, luminosity =  $2 \cdot 10^{31}$   $\text{cm}^{-2}\text{s}^{-1}$ ) was estimated to  $8.64 \cdot 10^4$  part/day.

## 4 Summary and outlook

The  $\Xi^-$  production reaction has been simulated as well as the most probable background sources. To reduce the background topological cuts have been defined and optimized. The calculated count rate expected for the upcoming experiment shows, that one can expect sufficient statistics.

Currently hardware and software for the HADES upgrade are in preparation. The Forward Detector is under construction and the first in-beam test with full size prototypes are scheduled for the beginning of 2019. The upcoming measurements of heavy ion collisions and reactions with pion beams will take place during the FAIR-Phase0 program. Finally, measurement of the proton-proton reaction, investigated in this work, should lead us to the pioneering observation of the multistrangeness production in elementary collisions.

**Acknowledgements:** This project has received funding from the European Union’s Horizon 2020 research and innovation programme under the Marie Skłodowska-Curie grant agreement No 665778 National Science Centre, Poland 2016/23/P/ST2/04066 POLONEZ.

## References

1. B. Abelev, et al. (ALICE Collaboration), Phys. Lett. B 728, 216 (2014)
2. B. Abelev, et al. (ALICE Collaboration), Phys. Rev. Lett. 111, 222301 (2013)
3. M. M. Aggarwal, et al. (STAR Collaboration), Phys. Rev. C 83, 024901 (2011)
4. J. Adams, et al. (STAR Collaboration), Phys. Rev. Lett. 98, 062301 (2007)
5. F. Antinori, et al. (NA57 Collaboration), Phys. Lett. B 595, 68 (2004)
6. C. Alt, et al. (NA49 Collaboration), Phys. Rev. C 78, 034918 (2008)

7. P. Chung, et al. (E895 Collaboration), *Phys. Rev. Lett.* 91, 202301 (2003)
8. K. Aamodt, et al. (ALICE Collaboration), *Eur. Phys. J. C* 71, 1594 (2011)
9. M. Agari (HERA-B), Ph.D. thesis, Universität Dortmund, [CERN-THESIS-2006-046, 2006 (unpublished)]
10. F. Antinori, et al. (NA57 Collaboration), *J. Phys. G* 32, 427 (2006)
11. G. Agakishiev, et al. (HADES Collaboration), *Phys. Rev. Lett.* 103, 132301 (2009)
12. G. Agakishiev, et al. (HADES Collaboration), *Phys. Rev. Lett.* 114, 212301 (2015)
13. Lie-Wen Chen, Che Ming Ko, Yiharn Tzeng, *Phys. Lett. B* 584, 269-275 (2004)
14. F. Li, et al., *Phys. Rev. C* 85, 064902 (2012)
15. G. Graef, J. Steinheimer, F. Li, M. Bleicher, *Phys. Rev. C* 90, 064909 (2014)
16. S. A. Bass, et al., *Prog. Part. Nucl. Phys.* 41, 255 (1998)
17. M. Bleicher, et al., *J. Phys. G* 25, 1859 (1999)
18. O. Buss, et al., *Phys. Rep.* 512, 1 (2012)
19. J. Weil, H. van Hees, and U. Mosel, *Eur. Phys. J. A* 48, 111 (2012)
20. S. Wheaton, J. Cleymans, and M. Hauer, *Comput. Phys. Commun.* 180, 84 (2009)
21. J. Steinheimer, and M. Bleicher, *J. Phys. G: Nucl. Part. Phys.* 43, 015104 (2016)
22. The HADES Collaboration, Agakichiev, G., Agodi, C. et al., *Eur. Phys. J. A* (2009) 41:243
23. J. Smyrski et al., *JINST* 13, P06009 (2018)
24. I. Frohlich et al., 2007 PoS ACAT2007 076 (Preprint 0708.2382)